# Quantification of Temperature-Dependent Charge Separation and Recombination Dynamics in Non-Fullerene Organic Photovoltaics

*Christopher C. S. Chan[#], Chao Ma[#], Xinhui Zou[#], Zengshan Xing, Guichuan Zhang, Hin-Lap Yip, Robert A. Taylor, Yan He, Kam Sing Wong*, and Philip C. Y. Chow**

[#] These authors contributed equally

Dr. C. C. S. Chan, Dr. C. Ma, Z. Xing, Prof. K. S. Wong
Department of Physics,
The Hong Kong University of Science and Technology, Clear Water bay, Kowloon, Hong Kong, P. R. China
E-mail: phkswong@ust.hk

X. Zou, Prof. Y. He
Department of Chemistry,
The Hong Kong University of Science and Technology, Clear Water bay, Kowloon, Hong Kong, P. R. China

Dr. G. Zhang, Prof. H-L. Yip
State Key Laboratory of Luminescent Materials and Devices,
Institute of Polymer Optoelectronic Materials and Devices, School of Materials Science and Engineering, South China University of Technology, 381 Wushan Road, 510640, Guangzhou, P. R. China

Prof. H-L. Yip
Department of Materials Science and Engineering,
City University of Hong Kong, Kowloon, Hong Kong, P. R. China

Prof. R. A. Taylor
Department of Physics,
Clarendon Laboratory, University of Oxford, Parks Road, Oxford OX1 3PU, UK.

Dr. C. C. S. Chan, Dr. P. C. Y. Chow
Department of Mechanical Engineering,
The University of Hong Kong, Pokfulam Road, Hong Kong. P. R. China
E-mail: pcyc@hku.hk

**Keywords:** organic photovoltaics, excitons, charge separation, ultrafast spectroscopy, charge recombination

**Abstract**

Transient optical spectroscopy is used to quantify the temperature-dependence of charge separation and recombination dynamics in P3TEA:SF-$PDI_2$ and PM6:Y6, two non-fullerene organic photovoltaic (OPV) systems with negligible driving force and high photocurrent quantum yields. By tracking the intensity of the transient electroabsorption (EA) response that arises upon interfacial charge separation in P3TEA:SF-$PDI_2$, a free charge generation rate constant of ~2.4 x $10^{10}$ $s^{-1}$ is observed at room temperature, with an average energy of ~230 meV stored between the interfacial charge pairs. Thermally-activated charge separation is also observed in PM6:Y6, and we estimate a faster charge separation rate of ~5.5 x $10^{10}$ $s^{-1}$ at room temperature, which is consistent with the higher device efficiency. When both blends are cooled down to cryogenic temperature, the reduced charge separation rate leads to increasing charge recombination either directly at the D/A interface or via the emissive singlet exciton state. A kinetic model is used to rationalize the results, showing that although photogenerated charges have to overcome a significant Coulomb potential to generate free carriers, OPV blends can achieve high photocurrent generation yields given that the thermal dissociation rate of charges outcompetes the recombination rate.

## 1. Introduction

Organic photovoltaics (OPVs) are flexible, lightweight, semi-transparent, printable and eco-friendly alternatives to silicon PV.[1] In contrast to inorganic materials, light absorption by organic materials does not directly generate free electrons and holes but instead creates Coulombically-bound electron-hole pairs (excitons).[2] A heterojunction between an electron-donating (donor) material and an electron-withdrawing (acceptor) material is used to partially separate the excitons into charge-transfer excitons (CTEs). It is well known that the energy offset between the exciton and CTE state provides a driving force for charge separation, and conventional OPV systems are designed with large interfacial energy offsets (typically ~200-250 meV).[3] However, overcoming the need for this energy offset is desirable because it reduces the CTE energy, thus leading to non-radiative recombination losses that limit the attainable open-circuit voltage ($V_{oc}$).[4]

Recent OPV systems based on non-fullerene acceptor molecules show near-unity IQEs with negligible charge separation driving force.[5–10] Despite the efficiency improvement, it remains unclear how electrons and holes overcome their mutual Coulomb attractions to separate into free charges without needing a driving force at the D/A interface. Many factors have been considered to play a role in enhancing interfacial charge separation, including molecular conformation,[11,12] vibrational coherence,[13] electrostatics,[14–16] energetic disorder[17] and dielectric constant,[18] among other properties. The close energy alignment and hybridization between the exciton and CTE states allow charges to regenerate singlet excitons from which they can recombine radiatively to the ground state (see **Figure 1a**). [2,8,19] This provides a pathway for reducing non-radiative recombination and leads to a higher $V_{oc}$.[8,19,20] Our recent work based on pump-push-probe transient absorption spectroscopy provides evidence that free carriers are generated upon thermal

activation of long-lived CTEs that takes over a hundred picoseconds to complete at room temperature.[21] This suggests that the CTEs need to overcome a significant Coulomb potential in order to separate into free carriers. On the other hand, another recent study has shown that the state-of-the-art non-fullerene OPV system (PM6:Y6) can achieve high photocurrent yields even at cryogenic temperatures (>50% at 125 K), thus indicating that charge separation is a barrierless process.[14]

Here we present a quantitative study on the temperature dependence of charge separation and charge recombination dynamics in two model non-fullerene OPV systems: P3TEA:SF-$PDI_2$ and PM6:Y6. We estimate the Coulomb binding energy of CTEs by extracting the time-dependent electroabsorption (EA) signal that arises due to local electric fields created during charge separation (Figure 1b). The charge separation rate is extracted as a function of temperature and shows thermal activation. Furthermore, the change in exciton emission yield with temperature is studied alongside the device photocurrent yield, revealing the temperature-dependent charge dynamics in these systems.

**2. Results**

We begin by studying the femtosecond transient absorption (TA) spectrum of P3TEA:SF-$PDI_2$ (see Methods for experimental details). As described in ref[7], P3TEA:SF-$PDI_2$ devices shows a high charge generation efficiency (IQE up to 85%) with negligible D/A energy offsets. The absorption spectra and chemical structures of P3TEA and SF-$PDI_2$ are shown in Figure 1c and d. **Figure 2a** shows the TA spectra of P3TEA:SF-$PDI_2$ at different time delays. At early times (<1ps) the TA spectrum shows a positive change in transmission between ~670-720 nm corresponding to the ground state bleach (GSB) P3TEA donor. We note that the TA response of excited states in

the SF-PDI$_2$ acceptor is much weaker than the donor polymer in the spectral region of interest, and can be neglected.[21] With increasing time delay, we observe a growth in a negative photo-induced absorption (PA) signal close to the optical edge leading to a spectral blue-shift. As discussed previously, as electron-hole pairs separate from the interfacial charge transfer (CTE) state, the local electric field between them causes an absorption shift that leads to an EA response, leading to the gradual spectral blue-shift in the TA signal (schematic in Figure 1b; the steady-state EA signal measured in a P3TEA:SF-PDI$_2$ device is overlaid on Figure 2a for comparison). [21] At low temperatures, we observe a reduced spectral blue-shift within the same timescale, with almost no spectral blue-shift seen at 10 K within a nanosecond (see Figure 2b; TA results for other temperatures are found in Figure S1 of the Supporting Information).

Extraction of the EA from the TA signal as a function of time can provide a precise measurement of the dynamics of free charge separation as well as the Coulomb potential that the charges have to overcome. [17,22–24] We use matrix decomposition to numerically extract the embedded EA kinetics from the TA data (see Supporting Information for details). As reported previously, the EA spectrum of the blend matches with the first derivative of its ground-state absorption and of the polymer GSB in the TA data (confirmed by steady-state device EA measurement; dashed line in Figure 2a and Figure S4 in the Supporting Information). [21] By determining the EA signal at various temperatures, we can numerically extract the kinetics of the EA from the TA data. We point out that the EA spectrum also changes with decreasing temperature due to the lowering of the optical gap. This is reflected in the red-shift of the polymer GSB in the TA data with decreasing temperature (shift by ~15 nm as the temperature is cooled down from 300 K to 10 K, see Figure

2a and b). This shift is accounted for in our EA extraction analysis (see details in Supporting Information).

Figure 2c shows the extracted EA kinetics at various temperatures. Since the growth in the EA signal is due to the Stark effect that arises from separating charge pairs, we can quantify the electric field between the charge pairs by calibrating it using the steady-state device EA spectrum measured under an applied electric field. This enables us to estimate the electrostatic energy stored in the electron-hole pairs, as reported in previous studies (see Supporting Information for details).[17,24] The calibrated EA kinetics are fitted to an exponential model: $E_{\max} \cdot [1 - \exp(-k_{\text{diss}}t)]$ , where $k_{\text{diss}}$ is the charge dissociation rate and $E_{\max}$ is the maximum average energy per charge pair when they are given sufficient time to dissociate. The best fit lines are shown in black in Figure 2c. At room temperature (300 K), we find that the average energy per charge pair rises with a rate constant of 2.4 x $10^{10}$ $s^{-1}$ until reaching a plateau at ~230 meV at ~200 ps. Since this system exhibits high IQE at room temperature (~85%),[7] this extracted value provides a reasonable estimate of the Coulomb potential that the charges have to overcome at the D/A interface in order to separate (see Fig 1a). Also, this value is comparable to the Coulomb binding energy of interfacial charge pairs found in other organic heterojunctions.[3,17,25,26]

The inset of Figure 2c plots the fitted $k_{\text{diss}}$ at various temperatures. We use the Arrhenius model to fit the extracted charge dissociation rates:

$$k_{\text{diss}} = A \exp\left(\frac{-E_{\text{a}}}{k_{\text{B}}T}\right),$$

where $k_{\text{B}}$ is the Boltzmann constant, $T$ is the temperature, $A$ is the frequency factor, and $E_{\text{a}}$ is the activation energy. The black line in the inset of Figure 2c shows the fit with $A$ = 4.5 x $10^{10}$ $s^{-1}$ and

$E_a$ = 17 meV. We note that the activation energy is not a direct measure of the CTE binding energy, but instead, it provides a measure of the interplay between charge dissociation and recombination rates at various temperatures. This explains why the activation energy is much smaller than the CTE binding energy determined above (over 200 meV), and it is comparable to the values measured by temperature-dependent photocurrent studies.[14,27] In addition to a lower $k_{diss}$, we find that $E_{max}$ is also reduced with decreasing temperature. $E_{max}$ is the maximum average energy per charge pair when they are given sufficient time to dissociate and avoid recombination. Therefore, the reduced $E_{max}$ at low temperature indicates that more charge pairs tend to recombine instead of separating.

We turn to time-resolved photoluminescence (PL) measurements (**Figure 3a**) to further study charge recombination in this blend. The blend PL lifetime increases with decreasing temperature, consistent with an increase in blend PL intensity measured at the same emission wavelength (see Figure S6 in Supporting Information). The emission energy of the blend is similar to the pure P3TEA polymer.[21] Due to the weak emission of the interfacial CTE state,[2] the blend emission is likely to arise from singlet excitons enabled by the negligible energy offset. Furthermore, as we reported previously,[28] this increase in blend emission at low temperature is not due to poor exciton diffusion towards the interface. Therefore, this increase in blend emission at low temperature is primarily caused by the increasing amount of charges that recombine radiatively via the emissive exciton state due to the reduced thermal separation rate of CTE into free carriers. This result is consistent with the reduced $E_{max}$ that we measured in the TA measurements. We note also that no additional blend PL is observed below 100 K, consistent with the similar $E_{max}$ at 10 K and 100 K (see Figure 3a and the red squares in Figure 3b). The more severe charge recombination at lower

temperature (greater blend PL and reduced $E_{max}$) is consistent with the reduced photovoltaic internal quantum efficiency (IQE), as shown in Figure 3b. With reducing temperature, we find a more significant drop in device IQE (with only ~3% of the charges extracted at 100 K) compared to the drop in $E_{max}$ from TA measurements. Although the TA measurement indicates that some charges do manage to separate at low temperatures ($E_{max} > 0$), we observe nearly no device IQE below 100 K. This is likely due to charge recombination that occurs in this blend beyond the temporal window of the TA measurement (1 ns). More discussions on the interplay between charge separation and recombination on the device IQE is found below.

We turn to study PM6:Y6, which shows an even higher IQE of >90%,[5] with an extended absorption into the near-infrared leading to higher power conversion efficiencies and similarly negligible interfacial energy offsets (absorption spectra chemical structure in Figure 1c and d). **Figure 4a** shows the TA spectra measured at various time delays at room temperature (298 K). An excitation wavelength of 800 nm is used to selectively generate photoexcitations in the Y6 acceptor phase (see Methods section for details). We attribute the positive ΔT/T signal at ~600 nm and ~850 nm to the GSB of the PM6 donor and the Y6 acceptor, respectively, and the negative ΔT/T signal at ~700-790 nm to the charge (polaron) PA signal [28] It is noted that both free charges and interfacial charges (CTE) can give rise to a similar PA signal in OPV blends, and therefore the PA signal kinetics may not necessarily represent the free charge generation dynamics.[22,24] For this blend, however, Wang et al. [29] have used transient and steady-state photo-induced absorption measurements to confirm that the charge PA signal in the 700-790 nm region can be assigned mainly to the charge-separated state (free charge carriers). We attempt to extract the EA signal that arises due to charge separation in this blend; however, unlike P3TEA:SF-PDI$_2$, there is a large

overlap between the EA signal and the other TA spectral features in PM6:Y6. This makes it difficult to reliably extract the EA signal embedded in the TA data. Additional discussions on TA spectral assignment and EA measurements are found in the Supporting Information.

Since the charge PA signal between ~700-790 nm can be assigned mainly to free charge carriers, [29] we study its kinetics to probe the charge generation dynamics in PM6:Y6 with respect to temperature. As detailed in our previous report,[28] by probing the temperature dependence on the GSB kinetics of PM6:Y6 at ~600 and ~850 nm (excited at 800 nm to create photoexcitations in the Y6 acceptor), we showed that the growth in the donor PM6 GSB at ~600 nm (associated with hole transfer at the interface) does not change as the temperature is decreased from 298 K to 15 K. However, the growth in the charge PA is significantly affected by temperature (temperature-dependent TA spectra shown in Figure S10). Figure 4b plots the kinetics of the charge PA signal from 1 ps onwards at various temperatures. The results clearly show the temperature dependence of the PA signal intensity, taking up to ~100 ps to maximize at room temperature. The maximum intensity of the PA signal ($PA_{max}$) within our temporal window (1 ns) shows a clear decrease with lowering temperature ($|\Delta T/T| \sim 1.8 \times 10^{-3}$ at room temperature to $\sim 0.8 \times 10^{-3}$ at 20 K), indicating that the population of free charges is decreased by approximately a factor of two. Similar to our analysis of P3TEA:SF-$PDI_2$ (see above), we estimate the rate of increase of the free charge population by applying an exponential fitting to the charge PA kinetics and obtain a growth rate of $k_{PA} \sim 5.5 \times 10^{10}$ $s^{-1}$ at room temperature. This rate is about a factor of two faster than the charge separation rate extracted for the P3TEA:SF-$PDI_2$ blend, which is consistent with the higher device efficiency in PM6:Y6 devices. Similar to P3TEA:SF-$PDI_2$, we observe a reduced charge PA growth rate and $PA_{max}$ in PM6:Y6 at decreasing temperature (see Figure 2c and 4b), thus

supporting the notion that free carrier generation is also a thermally-activated process in PM6:Y6. We note that the rate of charge separation ($k_{diss}$) for P3TEA:SF-PDI$_2$ is directly extracted through measuring the growth of the EA signal created as charge pairs separate, whereas for PM6:Y6 we extracted the charge separation rate directly from the charge PA kinetics ($k_{PA}$). Nevertheless, since the charge PA kinetics is mainly assigned to free carriers, we consider that $k_{PA}$ gives a reasonable estimate of the charge separation rate in PM6:Y6. The faster charge separation that we observe in PM6:Y6 compared to P3TEA:SF-PDI$_2$ could be due to the more efficient CTE separation facilitated by interfacial energy level bending[14,16], a larger electron delocalization,[30] and the formation of an excimer state that assists separation. [29]

Figure 4c shows the temperature-dependent time-resolved PL study performed on PM6:Y6 films. At room temperature, we observe fast PL decay (< 200 ps) close to our detection limit. This indicates that most photogenerated excitons can effectively separate into charges, in agreement with the high device efficiency. Similar to P3TEA:SF-PDI$_2$, with decreasing temperature, we observe a reduced PL decay rate and an increased PL intensity. We find similar PL emission energies for both blend and pure Y6 samples (see Figure S11 in Supporting Information). By comparing the PL of the blend and the pure Y6 samples under the same experimental conditions, we deduce that the PL ratio (ß = $PL_{blend}/PL_{pure}$) becomes larger at low temperature (i.e. less PL quenching). Since exciton dissociation into CTE is not significantly affected by temperature (as described by the GSB kinetics in the temperature-dependent TA data detailed in our previous work),[28] the reduced PL quenching reflects an increased amount of radiative charge recombination in the blend. Due to the small interfacial energy offset in the system, the increasing radiative charge recombination is likely to arise from the regeneration of the emissive singlet

excitons from bound electron-hole pairs in the CTE state, from which they can recombine radiatively to the ground state. [2,8,19]

Figure 4d plots the change in PL quenching (1 – β), the $PA_{max}$ value that we extracted from the TA experiment, and the external device photocurrent quantum yield (EQE) at various temperatures (normalized to the values at room temperature). Interestingly, we observe a very similar temperature dependence for all three parameters between 300K to 125K (dropping by ~35%). This result indicates that, at lowering temperature, an increasing population of charges remain bound at the interface (CTE) and therefore do not separate into free charges to form photocurrent. Instead, these bound charges tend to recombine to the ground state, either directly at the interface (CTE to ground state transition; largely non-radiative) [31] or via the emissive singlet exciton state through repopulation from the CTE), [2,8,19] both of which give rise to a faster PL decay. It is important to note that the regenerated excitons are not necessarily lost, but can either again dissociate into CTE (and subsequently free charges if there is sufficient thermal energy) or decay to the ground state.[21] The same applies to the regenerated CTE following bimolecular free carrier encounters at the interface.[32] At room temperature, most photogenerated electron-hole pairs manage to thermalize into free carriers and generate photocurrent at short-circuit condition, as evidenced by the strong PL quenching and high device photocurrent values.

**3. Discussions**

We rationalize our results using a kinetic model. [33,34] Suppose that *G* is the generation rate of bound electron-hole pairs (excitons and CTE), *R* is the rate of bimolecular free charge encounters

that regenerates bound charges and $k_{rec}$ is the overall recombination rate of bound charges, then the change in the population density of bound charges ($X$) in time is given by

$$\frac{dX}{dt} = G - k_{rec}X - k_{diss}X + R.$$

It can be shown that the net generation rate of free carriers in steady-state becomes

$$U = PG - (1 - P)R,$$

where $P = k_{diss}/(k_{diss} + k_{rec})$ is the probability of free charge generation given by the interplay between dissociation and recombination rates at thermodynamic equilibrium.[33] In a working device where charges are extracted, the free charge generation yield ($U$) is greater than zero and scales with $P$. When $k_{diss} >> k_{rec}$, $P$ tends to unity, and free charge generation is maximized. This is the case near room temperature for both P3TEA:SF-PDI$_2$ and PM6:Y6 blends, but the faster $k_{diss}$ in the latter is consistent with the higher device IQE and PL quenching. With lowering temperature, $k_{diss}$ is reduced, and therefore $P$ is lowered, leading to lower free charge generation yield for both blends. We point out that the temperature-dependence of $U$ does not only scale with $k_{diss}$, since $k_{rec}$ and $R$ are also likely to be lowered with decreasing temperature (slower vibrational relaxation for $k_{rec}$,[35] and lower charge mobilities at reduced temperature for $R$).[33] Therefore, the precise temperature dependence of free charge generation yield for a given material system depends on the interplay between these rates. Despite the slow $k_{diss}$ in NFA blends with negligible D/A offset (~3 orders of magnitude slower compared to fullerene blends with large offsets at room temperature),[21] high photocurrent yields can still be achieved provided that $k_{rec}$ is sufficiently slow compared to $k_{diss}$. Furthermore, although $k_{diss}$ is reduced with decreasing temperature, high charge separation yields can still be achieved provided that $k_{rec}$ maintains slower than $k_{diss}$, such that the bound electron-hole pairs have sufficient time to thermalize into free carriers.[32] The higher $k_{diss}/k_{rec}$ ratio in PM6:Y6 compared to P3TEA:SF-PDI$_2$ is the likely reason for the more

efficient photocurrent generation at both room temperature and at lower temperatures (despite the fact that free charge generation is thermally activated in both systems). This is supported by our experimental results showing faster $k_{diss}$ for PM6:Y6 compared to P3TEA:SF-PDI$_2$ (by about a factor of two). Furthermore, we consider that slower $k_{rec}$ in PM6:Y6 is also a key factor for allowing efficient charge generation, and this is likely related to the longer-lived interfacial and local excited states in Y6 molecules that extends into the nanosecond timescale.[29,30,36]

In conclusion, we performed time-resolved optical measurements to quantify charge dynamics in NFA-OPV with negligible interfacial energy offset (P3TEA:SF-PDI$_2$ and PM6:Y6). Our results show that free charge generation requires thermal activation in both blends. By extracting the EA signal that arises during charge separation in P3TEA:SF-PDI$_2$, we measure a dissociation rate of ~2.4 x $10^{10}$ $s^{-1}$ at room temperature and a Coulomb barrier of ~230 meV at the interface. For PM6:Y6, we observe a faster charge dissociation rate of ~5.5 x $10^{10}$ $s^{-1}$ through probing the charge PA signal in PM6:Y6. For both systems, a slower charge dissociation rate is measured at lower temperature and more charges tend to recombine back to the ground state, either directly at the interface (CTE to ground state transition; largely non-radiative) or via the emissive singlet exciton state (as evidenced by the increasing PL; ~50-70% at 100 K). Although charge separation rate scales with increasing temperature, a high free charge generation yield can still be achieved at low temperature provided that the charge recombination rate is sufficiently slow (i.e. $k_{diss} > k_{rec}$). Therefore, to minimize recombination losses in OPV devices, focus should be placed on extending the lifetimes of the interfacial charge pairs and the localized excited states in the lower gap component (either donor or acceptor material).

## 4. Experimental Methods

Thin-film and device preparation

P3TEA, SF-$PDI_2$, PM6 and Y6 were synthesized as reported in previous work.[5,7] P3TEA:SF-$PDI_2$ solutions were prepared with 1:1.5 donor to acceptor weight ratio and dissolved in 1,2,4-trimethylbenzene (TMB) with 2.5% of 1,8-octanedithiol (ODT) at 9 mg $mL^{-1}$. PM6:Y6 solutions were prepared at weight ratio of 1:1.2 in chloroform (CF) with 0.5% of 1-chloronaphthalene (CN), and at a total concentration of 16 mg $mL^{-1}$. The solutions were left for stirring at 100 °C for at least 1 hour prior to film deposition. Pre-patterned ITO-coated glass substrates (with a sheet resistance of 15 Ω per square) and quartz substrates were cleaned by sonicating in deionized water, acetone, and isopropanol for 30 minutes successively, followed by UV/ozone treatment for 60 minutes. A ZnO electron transport layer was spin-coated onto the ITO glass at 5000 r.p.m. from a ZnO precursor solution. For optical measurements, organic thin-films were prepared by spin-coating the solutions onto quartz in a $N_2$ filled glove box. For device samples, the films were spin-coated onto ITO/ZnO glass, and a thin layer of PNDI was deposited as the anode interlayer followed by deposition of 15 nm of silver as the top electrode (at a vacuum level of $3 \times 10^{-6}$ torr). Each device pixel had an area of 5.9 $mm^2$, and all samples were encapsulated using epoxy and glass inside the glovebox to avoid degradation during measurements.

Steady-state optical and electrical measurements

Ultraviolet-visible absorption spectra were obtained using a Perkin Elmer Lambda 20 UV/VIS Spectrophotometer. Steady-state electroabsorption (EA) spectrum was determined by measuring the relative change in transmission ($\Delta T/T$) through the semi-transparent, ultrathin (15 nm) silver electrode at various wavelengths in response to a varying electric field applied across the device

electrodes. The device was held under a small (-1 V) reverse bias to minimize charge injection from the electrodes. Device photocurrent measurements were measured under simulated AM1.5G illumination from a Newport lamp, calibrated using a standard Si diode (with a KG5 filter, purchased from PV Measurement) to bring spectral mismatch to unity, and a metal mask with an aperture aligned with the device area was used during measurements. The device was connected inside a nitrogen cryostat for low-temperature photocurrent measurements.

Transient absorption spectroscopy

Two beams were split from the 800 nm output of a Ti:Sapphire laser amplifier (Coherent Legend Elite, repetition rate of 1 kHz, 100fs). One of the split outputs is used to photoexcite the sample either directly at 800 nm or at other wavelengths generated in an optical parametric amplifier (Coherent OPerA Solo). The other split output generates a white light continuum probe pulse by focusing the beam onto a sapphire plate. The optical pulses were spatially overlapped in the encapsulated thin-film sample placed inside a helium cryostat, and temporally delayed using a motor-driven delay stage. The probe was guided into a spectrometer (Acton instruments SpectraPro 275) with a 50 LP/mm grating and detected by a Silicon array detector. The pump-induced change in transmission ($\Delta T/T$) was recorded shot by shot. The pump fluence was set at ~3.5 μJ $cm^{-2}$ per pulse. Background signals such as PL and laser scatter were subtracted from the signal. For the PM6:Y6 study, a pump of 800 nm selectively photoexcites the Y6 acceptor component. To pump the P3TEA:SF-$PDI_2$, a 500 nm pump pulse was generated by the OPA to excite the acceptor. (see Figure 1c for the relative absorption of the materials). Temperature artefacts were characterized by performing pump fluence dependent TA studies. We rule out the

influence of thermal artefacts on our analysis since we do not observe any clear fluence dependence on the TA spectral evolution (see Supporting Information for details).

Time-resolved photoluminescence spectroscopy

Measurements were carried out on encapsulated thin-films. For the Y6 and PM6:Y6, a 100 fs Ti:Sapphire oscillator (Coherent Mira 900) operating at 8 MHz repetition rate was tuned to 840 nm and focused to excite the sample. The PL was collected and guided to an InGaAs photon counter passing through a 900 nm long-pass luminescence filter to carry out time-correlated single-photon counting (TCPSC), integrating the majority of the PL. Low-temperature measurements were carried out with the sample mounted inside a helium flow cryostat with an active feedback temperature controller. The P3TEA:SF-$PDI_2$ samples were photoexcited using the 710 nm output of an oscillator laser running at 76 MHz. For the visible/NIR measurements, the photoluminescence was collected and guided into a spectrometer equipped with a silicon single-photon counter to measure the PL decay (probed at 820 nm). The PL spectrum is measured using a silicon photodiode array detector.

**Supporting Information**

Supporting Information is available from the Wiley Online Library or from the author.

**Acknowledgements**

The authors thank funding support by the Hong Kong Research Grants Council (project numbers 16306117, 16304218, 16306319, 16302520, AoE/P-02/12, R6021-18 and C6023-19) and William Mong Institute of Nano Science and Technology (project number WMINST19/SC04). P. C. Y. C.

acknowledges funding support from Faculty of Engineering and University Research Committee (The University of Hong Kong), and Open Fund of the State Key Laboratory of Luminescent Materials and Devices (South China University of Technology). H-L. Y. acknowledges funding support from the Guangdong Major Project of Basic and Applied Basic Research (No. 2019B030302007). Special thanks go to Kwok Fai Yeung for providing technical support.

**Conflict of Interest**

The authors declare no competing interests

**References**

[1] G. Zhang, J. Zhao, P. C. Y. Chow, K. Jiang, J. Zhang, Z. Zhu, J. Zhang, F. Huang, H. Yan, *Chem. Rev.* **2018**, *118*, 3447.

[2] V. Coropceanu, X.-K. Chen, T. Wang, Z. Zheng, J.-L. Brédas, *Nat. Rev. Mater.* **2019**, *4*, 689.

[3] T. M. Clarke, J. R. Durrant, *Chem. Rev.* **2010**, *110*, 6736.

[4] K. Vandewal, K. Tvingstedt, A. Gadisa, O. Inganäs, J. V Manca, *Nat. Mater.* **2009**, *8*, 904.

[5] J. Yuan, Y. Zhang, L. Zhou, G. Zhang, H.-L. Yip, T.-K. Lau, X. Lu, C. Zhu, H. Peng, P. A. Johnson, M. Leclerc, Y. Cao, J. Ulanski, Y. Li, Y. Zou, *Joule* **2019**, *3*, 1140.

[6] D. Baran, T. Kirchartz, S. Wheeler, S. Dimitrov, M. Abdelsamie, J. Gorman, R. S. Ashraf, S. Holliday, A. Wadsworth, N. Gasparini, P. Kaienburg, H. Yan, A. Amassian, C. J. Brabec, J. R. Durrant, I. McCulloch, *Energy Environ. Sci.* **2016**, *9*, 3783.

[7] J. Liu, S. Chen, D. Qian, B. Gautam, G. Yang, J. Zhao, J. Bergqvist, F. Zhang, W. Ma, H. Ade, O. Inganäs, K. Gundogdu, F. Gao, H. Yan, *Nat. Energy* **2016**, *1*, 16089.

[8] D. Qian, Z. Zheng, H. Yao, W. Tress, T. R. Hopper, S. Chen, S. Li, J. Liu, S. Chen, J. Zhang, X. Liu, B. Gao, L. Ouyang, Y. Jin, G. Pozina, I. A. Buyanova, W. M. Chen, O. Inganäs, V. Coropceanu, J. Bredas, H. Yan, J. Hou, F. Zhang, A. A. Bakulin, F. Gao, *Nat. Mater.* **2018**, *17*, 703.

[9] C. Li, J. Zhou, J. Song, J. Xu, H. Zhang, X. Zhang, J. Guo, L. Zhu, D. Wei, G. Han, J. Min, Y. Zhang, Z. Xie, Y. Yi, H. Yan, F. Gao, F. Liu, Y. Sun, *Nat. Energy* **2021**, *6*, 605.

[10] Y. Zhong, M. Causa', G. J. Moore, P. Krauspe, B. Xiao, F. Günther, J. Kublitski, R. Shivhare, J. Benduhn, E. BarOr, S. Mukherjee, K. M. Yallum, J. Réhault, S. C. B.

Mannsfeld, D. Neher, L. J. Richter, D. M. DeLongchamp, F. Ortmann, K. Vandewal, E. Zhou, N. Banerji, *Nat. Commun.* **2020**, *11*, 1.

[11] N. A. Ran, S. Roland, J. A. Love, V. Savikhin, C. J. Takacs, Y.-T. Fu, H. Li, V. Coropceanu, X. Liu, J.-L. Brédas, G. C. Bazan, M. F. Toney, Di. Neher, T.-Q. Nguyen, *Nat. Commun.* **2017**, *8*, 79.

[12] X.-K. Chen, M. K. Ravva, H. Li, S. M. Ryno, J.-L. Brédas, *Adv. Energy Mater.* **2016**, *6*, 1601325.

[13] Y. Song, S. N. Clafton, R. D. Pensack, T. W. Kee, G. D. Scholes, *Nat. Commun.* **2014**, *5*, 4933.

[14] L. Perdigón-Toro, H. Zhang, A. Markina, J. Yuan, S. M. Hosseini, C. M. Wolff, G. Zuo, M. Stolterfoht, Y. Zou, F. Gao, D. Andrienko, S. Shoaee, D. Neher, *Adv. Mater.* **2020**, *32*, 1906763.

[15] H. Yao, Y. Cui, D. Qian, C. S. Ponseca, A. Honarfar, Y. Xu, J. Xin, Z. Chen, L. Hong, B. Gao, R. Yu, Y. Zu, W. Ma, P. Chabera, T. Pullerits, A. Yartsev, F. Gao, J. Hou, *J. Am. Chem. Soc.* **2019**, *141*, 7743.

[16] S. Karuthedath, J. Gorenflot, Y. Firdaus, N. Chaturvedi, C. S. P. De Castro, G. T. Harrison, J. I. Khan, A. Markina, A. H. Balawi, T. A. Dela Peña, W. Liu, R.-Z. Liang, A. Sharma, S. H. K. Paleti, W. Zhang, Y. Lin, E. Alarousu, D. H. Anjum, P. M. Beaujuge, S. De Wolf, I. McCulloch, T. D. Anthopoulos, D. Baran, D. Andrienko, F. Laquai, *Nat. Mater.* **2021**, *20*, 378.

[17] S. M. Menke, A. Cheminal, P. Conaghan, N. A. Ran, N. C. Greehnam, G. C. Bazan, T.-Q. Nguyen, A. Rao, R. H. Friend, *Nat. Commun.* **2018**, *9*, 277.

[18] B. Bernardo, D. Cheyns, B. Verreet, R. D. Schaller, B. P. Rand, N. C. Giebink, *Nat. Commun.* **2014**, *5*, 3245.

[19] F. D. Eisner, M. Azzouzi, Z. Fei, X. Hou, T. D. Anthopoulos, T. J. S. Dennis, M. Heeney, J. Nelson, *J. Am. Chem. Soc.* **2019**, *141*, 6362.

[20] X.-K. Chen, V. Coropceanu, J.-L. Brédas, *Nat. Commun.* **2018**, *9*, 5295.

[21] T. F. Hinrichsen, C. C. S. Chan, C. Ma, D. Paleček, A. Gillett, S. Chen, X. Zou, G. Zhang, H.-L. Yip, K. S. Wong, R. H. Friend, H. Yan, A. Rao, P. C. Y. Chow, *Nat. Commun.* **2020**, *11*, 5617.

[22] M. Causa', J. De Jonghe-Risse, M. Scarongella, J. C. Brauer, E. Buchaca-Domingo, J.-E. Moser, N. Stingelin, N. Banerji, *Nat. Commun.* **2016**, *7*, 12556.

[23] K. N. Schwarz, P. B. Geraghty, V. D. Mitchell, S.-U.-Z. Khan, O. J. Sandberg, N. Zarrabi, B. Kudisch, J. Subbiah, T. A. Smith, B. P. Rand, A. Armin, G. D. Scholes, D. J. Jones, K. P. Ghiggino, *J. Am. Chem. Soc.* **2020**, *142*, 2562.

[24] S. Gelinas, A. Rao, A. Kumar, S. L. Smith, A. W. Chin, J. Clark, T. S. van der Poll, G. C. Bazan, R. H. Friend, *Science* **2014**, *343*, 512.

[25] S. Gélinas, O. Paré-Labrosse, C. N. Brosseau, S. Albert-Seifried, C. R. McNeill, K. R.

Kirov, I. A. Howard, R. Leonelli, R. H. Friend, C. Silva, *J. Phys. Chem. C* **2011**, *115*, 7114.

[26] S. Athanasopoulos, F. Schauer, V. Nádaždy, M. Weiß, F.-J. Kahle, U. Scherf, H. Bässler, A. Köhler, *Adv. Energy Mater.* **2019**, *9*, 1900814.

[27] F. Gao, W. Tress, J. Wang, O. Inganäs, *Phys. Rev. Lett.* **2015**, *114*, 128701.

[28] C. Ma, C. C. S. Chan, X. Zou, H. Yu, J. Zhang, H. Yan, K. S. Wong, P. C. Y. Chow, *Sol. RRL* **2021**, *5*, 2000789.

[29] R. Wang, C. Zhang, Q. Li, Z. Zhang, X. Wang, M. Xiao, *J. Am. Chem. Soc.* **2020**, *142*, 12751.

[30] G. Zhang, X.-K. Chen, J. Xiao, P. C. Y. Chow, M. Ren, G. Kupgan, X. Jiao, C. C. S. Chan, X. Du, R. Xia, Z. Chen, J. Yuan, Y. Zhang, S. Zhang, Y. Liu, Y. Zou, H. Yan, K. S. Wong, V. Coropceanu, N. Li, C. J. Brabec, J.-L. Bredas, H.-L. Yip, Y. Cao, *Nat. Commun.* **2020**, *11*, 3943.

[31] L. Perdigón-Toro, L. Q. Phuong, S. Zeiske, K. Vandewal, A. Armin, S. Shoaee, D. Neher, *ACS Energy Lett.* **2021**, *6*, 557.

[32] T. M. Burke, S. Sweetnam, K. Vandewal, M. D. McGehee, *Adv. Energy Mater.* **2015**, *5*, 1500123.

[33] L. J. A. Koster, E. C. P. Smits, V. D. Mihailetchi, P. W. M. Blom, *Phys. Rev. B* **2005**, *72*, 1.

[34] C. L. Braun, *J. Chem. Phys.* **1984**, *80*, 4157.

[35] V. Coropceanu, X.-K. Chen, T. Wang, Z. Zheng, J.-L. Brédas, *Nat. Rev. Mater.* **2019**, *4*, 689.

[36] A. Classen, C. L. Chochos, L. Lüer, V. G. Gregoriou, J. Wortmann, A. Osvet, K. Forberich, I. McCulloch, T. Heumüller, C. J. Brabec, *Nat. Energy* **2020**, *5*, 711.

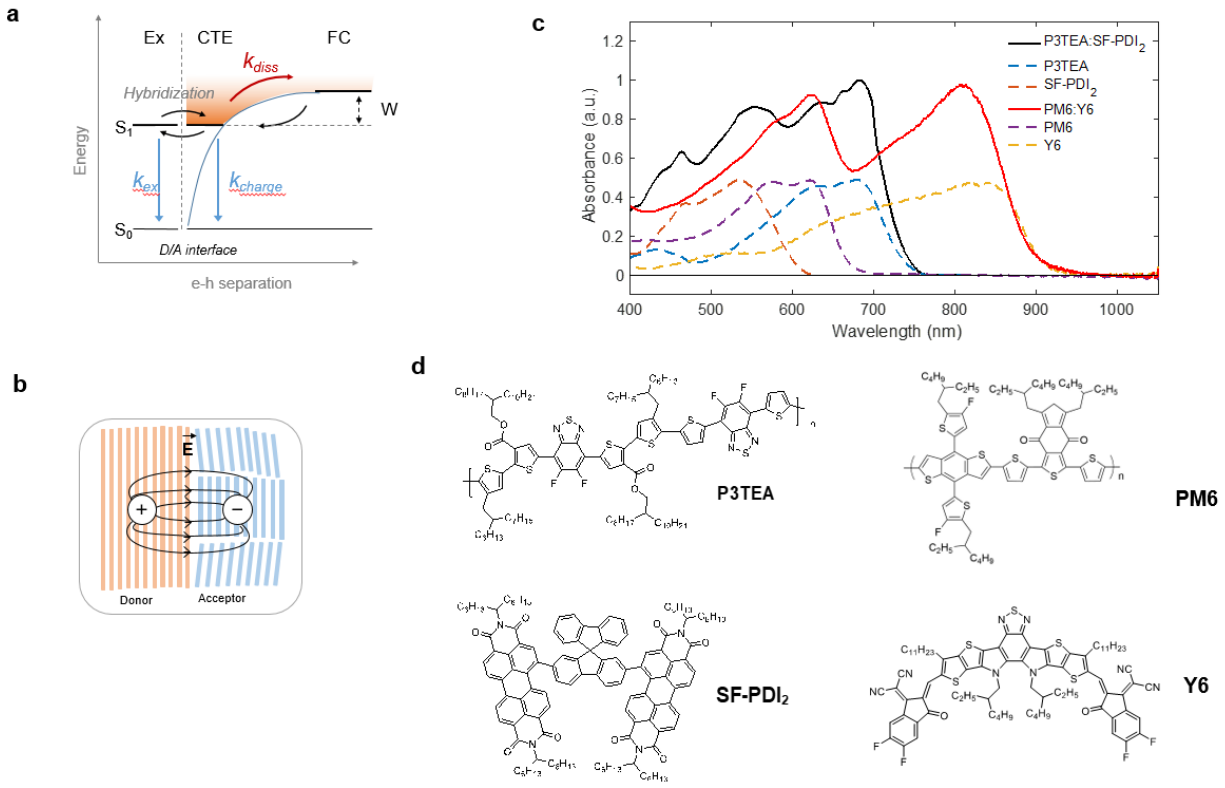


**Figure 1.** Charge photogeneration processes and material system. (a) Schematic illustrations of charge separation processes in organic photovoltaics with negligible interfacial energy offsets. The close energy alignment between lowest energy local excitons (Ex) and interfacial charge-transfer excitons (CTEs) leads to state hybridization. Interfacial CTEs must overcome a Coulomb potential (W) in order to thermally separate into free charge carriers (FC) at a rate of $k_{diss}$. Charges that fail to separate will recombine to the electronic ground state either directly at the D/A interface ($k_{charge}$) or via the emissive exciton state ($k_{ex}$), both contributing to the overall recombination rate ($k_{rec}$). (b) The dipolar electric field generated between the separated electron and hole causes a Stark shift of the absorption spectrum, leading to a transient electroabsorption (EA) response near the optical edge during interfacial charge separation. (c) Absorption spectra of pristine films of P3TEA, SF-PDI$_2$, PM6, Y6 in dashed lines and their respective blends in solid lines. (d) Chemical structure of

donor polymer P3TEA, small molecule acceptor SF-PDI$_2$; and donor polymer PM6 as well as small molecule acceptor Y6

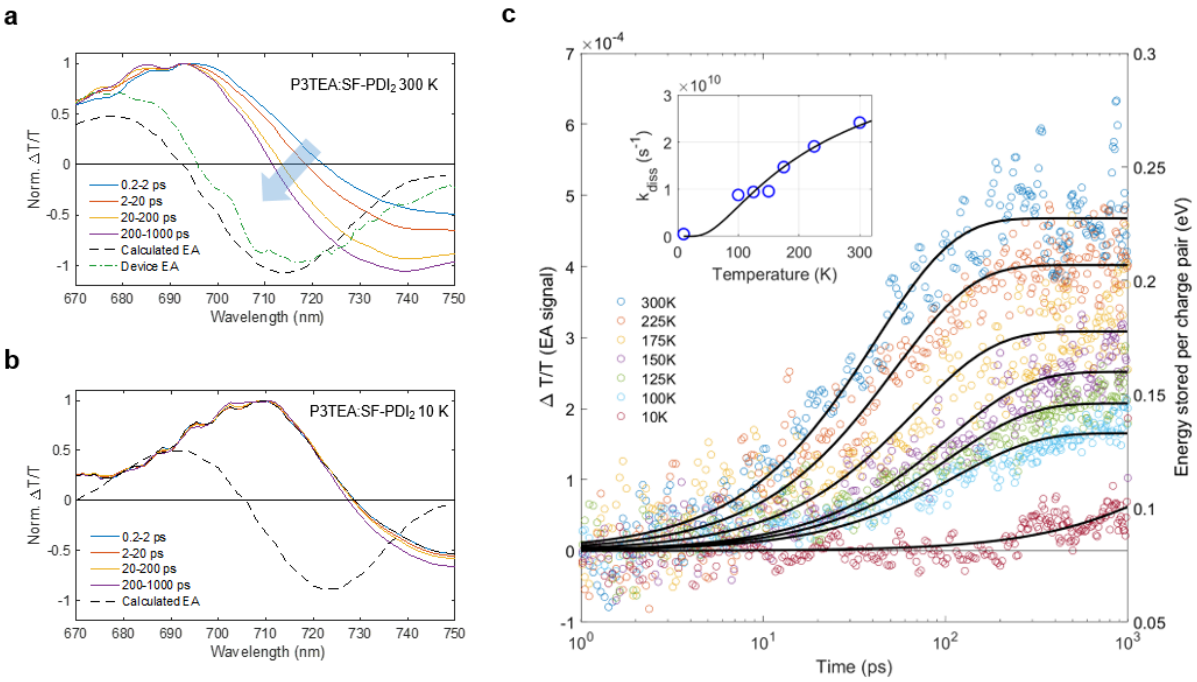


**Figure 2.** Quantifying charge generation in P3TEA:SF-PDI$_2$. (a, b) Normalized transient absorption (TA) spectroscopy measurements of P3TEA:SF-PDI$_2$ film at 300 K and 10 K, respectively. The samples were photoexcited at 500 nm with a pulse fluence of ~3.5 μJ cm$^{-2}$ (see Supporting Information for additional TA data on this system). The steady-state device EA is measured in a diode structure under an applied bias (dashed green line in panel (a); see Methods and SI for details). We find that the measured device EA spectrum is in agreement with the first derivative of the ground state absorption of the early time (<1 ps) TA spectrum (dashed black line; also see Figure S4 in the SI). (c) Kinetics of the local electroabsorption (EA) response at various temperatures numerically extracted from the TA data (see Supporting Information for details). The intensity of the transient EA response was calibrated using device EA to determine the energy stored in the dipolar electric field generated by the separated electron-hole pairs. The fitted lines represent exponential fits based on the exponential model as described in the main text: $E_{\max} \cdot [1 - \exp(-k_{\text{diss}} t)]$, where $k_{\text{diss}}$ is the charge separation rate and $E_{max}$ is the maximum average

energy per charge pair. Insert shows the relationships of $k_{diss}$ and $E_{max}$ with temperature, and the fitted line shows Arrhenius fit with $A$ = 4.5 x $10^{10}$ $s^{-1}$ and $E_a$ = 17 meV.

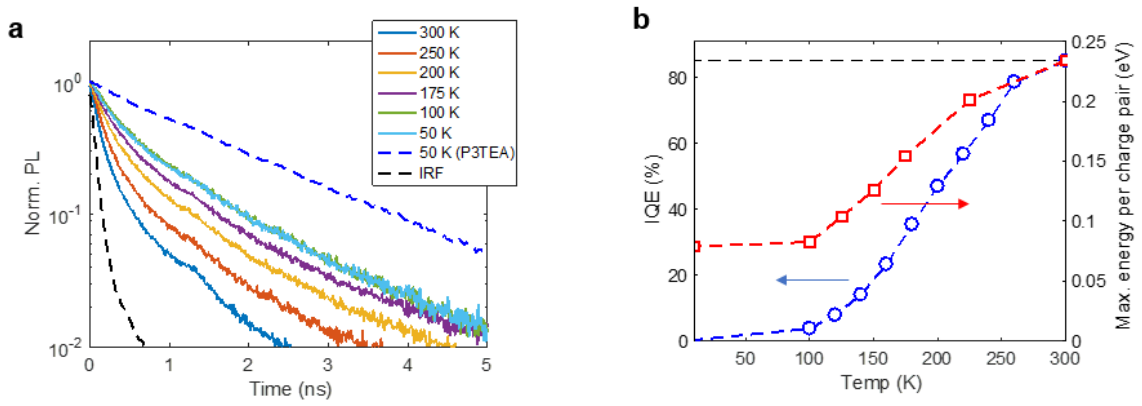


**Figure 3.** (a) Time-resolved photoluminescence (TRPL) decay measurements of P3TEA:SF-PDI$_2$ film at various temperatures, all photoexcited at 710 nm and probed at 820 nm. The reduced decay rate from 300 K to 100 K is consistent with the increased PL intensity over the same temperature range (see Figure S6 in Supporting Information). The blue and black dotted lines show PL decay of pure P3TEA film at 50 K and the instrument response function (IRF), respectively. (b) Comparison of P3TEA:SF-PDI$_2$ device internal quantum yield (IQE) with the maximum energy per charge pair ($E_{max}$) determined from transient absorption measurements shown in Figure 2.

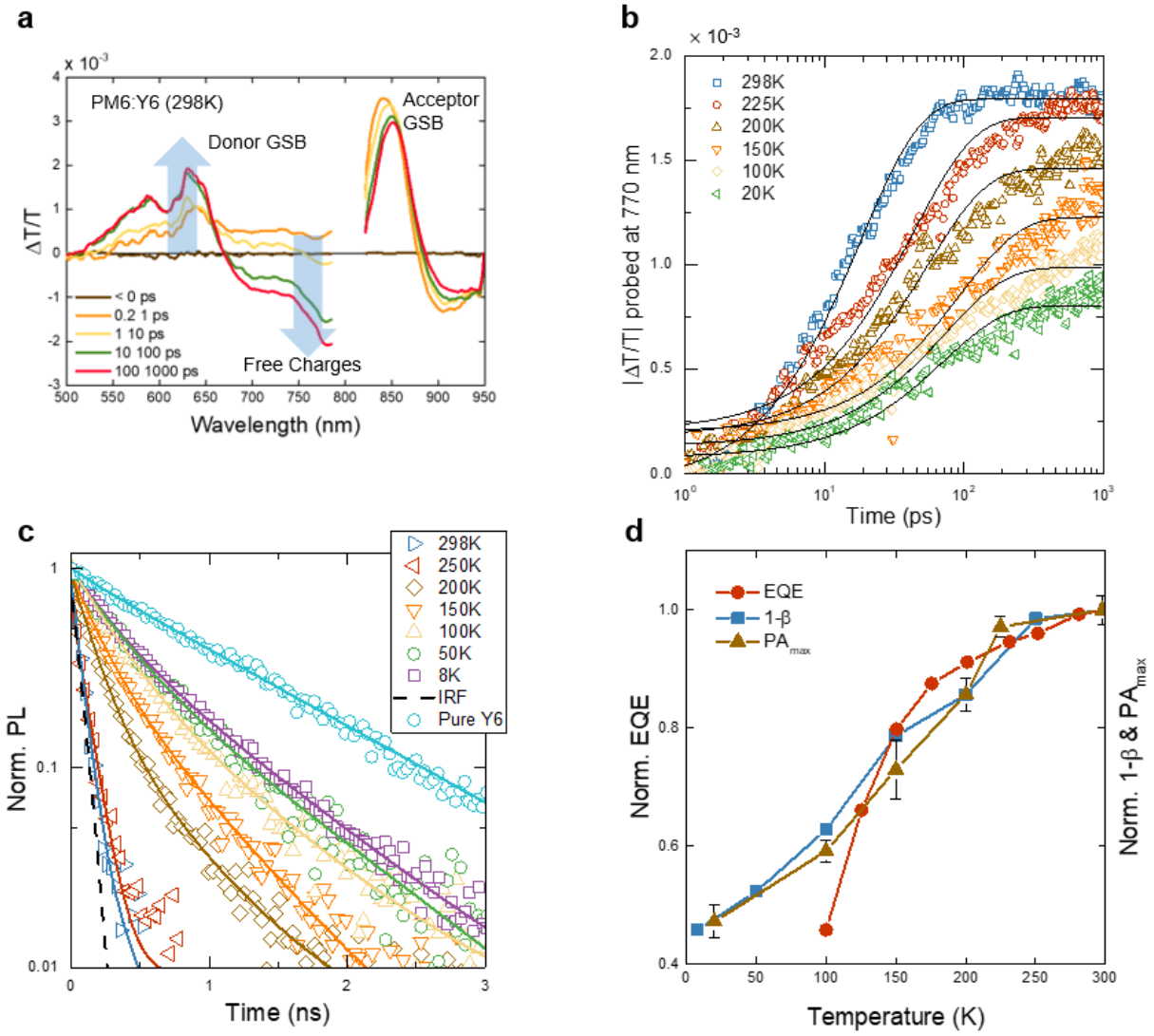


**Figure 4.** Transient absorption spectroscopy and tracking the charge generation in PM6:Y6. (a) TA spectra of PM6:Y6 excited selectively into the acceptor at 800 nm showing growth in the donor GSB due to charge transfer into the donor,[28] and growth in the PA associated with the charge-separated state (free charge carriers) in the ~10-100 ps timescale.[29] (b) Transient absorption kinetics probed at ~770 nm at different temperatures. As formulated in the main text and previous reports,[29] the growing PA in this spectral region is a signature for free charge generation. (c) Normalized time-resolved photoluminescence (TRPL) of PM6:Y6 film at various temperatures, with the dashed line showing the instrument response function (IRF). TRPL of pure Y6 film is

found in Figure S11 in the Supporting Information. Taking the normalized area under the TRPL trace for both PM6:Y6 blend and pure Y6 allows us to compare their respective PL intensity at each temperature (i.e. PL ratio: ß = $PL_{blend}/PL_{pure}$). The PL quenching in the blend versus pure film is given by one minus ß. (d) Comparison of the temperature dependence of the PL quenching (1- ß), the device EQE (obtained from Ref. [14]), and the maximum intensity of the charge PA ($PA_{max}$; error bars from uncertainty in TA measurement) all normalized at room temperature. The reduced PL quenching at low-temperature matches with the drop in device photocurrent yield. The $PA_{max}$ decrease with temperature is well correlated to the decreasing PL quenching.

**Table of Contents**

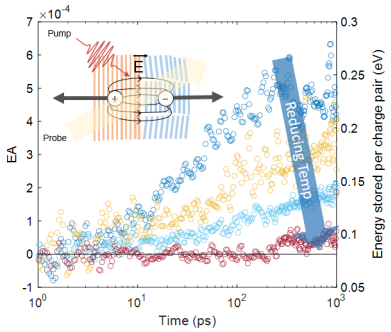


In this work, transient optical spectroscopy methods are used to quantify the temperature-dependence of charge generation dynamics in efficient non-fullerene organic photovoltaic blends with negligible driving force. The results show that the photogenerated electron-hole pairs can thermally separate at the D/A interface, given that they are sufficiently long-lived (even at a reduced temperature for state-of-the-art materials).